The Astrophysical Journal Letters, 953:L14 (6pp), 2023 August 10 https://doi.org/10.3847/2041-8213/ace88b

Possible Detection of the Progenitor of the Type II Supernova SN 2023ixf

Joanne L Pledger[1] and Michael M Shara[2]
[1] Jeremiah Horrocks Institute, University of Central Lancashire, Preston, PR1 2HE, UK; jpledger@uclan.ac.uk
[2] American Museum of Natural History, New York City, NY 10024, USA
Received 2023 May 23; revised 2023 July 11; accepted 2023 July 17; published 2023 August 14

Abstract

Stellar evolution theory predicts multiple pathways to the explosive deaths of stars as supernovae. Locating and characterizing the progenitors of well-studied supernovae is important to constrain the theory and to justify and design future surveys to improve on progenitor detections. Here we report the serendipitous preexplosion imaging, by the Hubble Space Telescope, of SN 2023ixf, one of the nearest extragalactic supernovae ever discovered, in the galaxy M101. The extremely red color and absolute magnitude $M_{\rm F814W} = -5.11^{+0.65}_{-0.47}$ mag suggest that the progenitor was a red supergiant. Comparison with stellar evolutionary isochrones suggests it is within the relatively low initial mass range of ∼8–10 $M_{\odot}$ and that there is likely a lot of dust present at the supernova site.

Unified Astronomy Thesaurus concepts: Type II supernovae (1731); Supernovae (1668); Core-collapse supernovae (304)

1. Introduction

Supernovae are responsible for the production of many of the chemical elements and dust in galaxies and throughout the Universe (Burbidge et al. 1957; Cameron 1957; Hoyle & Wickramasinghe 1970; Johnson et al. 2020), the heating of the interstellar medium and galactic fountains (McKee & Cowie 1975; Corbelli & Salpeter 1988), cosmic rays (Baade & Zwicky 1934; Blandford & Ostriker 1978), long-duration gamma-ray bursts (Cano et al. 2017), and possibly even the formation of our own solar system (Clayton 1982). They are the most luminous distance indicators known, responsible for the detection of the dark energy (Riess et al. 1998; Perlmutter et al. 1999). Understanding how supernovae come about is thus important to almost every field in astrophysics. The most basic question that must be answered to make progress in understanding supernovae is: Which stars become supernovae?

Nearly 50 years ago Beatrice Tinsley (Tinsley 1975) posed that question and summarized everything then known about the subject in an 11 page review article. In the interim over 5600 refereed journal articles have greatly advanced both observations and stellar evolution theory to yield some answers, but half a century later there are still multiple types of supernovae for which the answer remains "We still do not know for certain." This ignorance is a major impediment to testing theories of the late stages of stellar evolution in both single and binary stars (Smartt 2009; Langer 2012; Sukhbold et al. 2016; Williams et al. 2019; Rodríguez 2022; Liu et al. 2023).

To date there have been ∼30 direct detections of Type II supernova (SN II) progenitors (see Van Dyk 2017 for a review), the first being supernova (SN) 1961V in NGC 1058 (Bertola 1964; Zwicky 1964) and the closest being SN 1987A in the Large Magellanic Cloud (Gilmozzi et al. 1987). Many pre-SN observations only yield an upper limit; successful detections of progenitors are typically limited to ∼30 Mpc. At a distance of just 6.4 Mpc (Shappee & Stanek 2011) SN 2023ixf in M101 is one of the closest and brightest extragalactic supernovae ever detected. Intensive follow-up studies at many wavelengths are underway, in the X-ray (Grefenstette 2023; Kawai et al. 2023) and optical (Villafane et al. 2023), and also a hunt for the associated neutrinos (Thwaites et al. 2023). This will be one of the most intensively studied supernovae ever, thus characterizing its progenitor is clearly of importance.

SN 2023ixf in M101 was discovered by K. Itagaki on 2023 May 19 with a position of α(J2000) = 14:03:38.564 and δ (J2000) = 54:18:42.02 (Itagaki 2023) and was classified as an SN II shortly after by Perley et al. (2023). In this Letter we use archival Hubble Space Telescope (HST) Advanced Camera for Surveys (ACS)/Wide Field Camera (WFC) imaging to identify the possible progenitor of this event and use evolutionary models to predict an initial mass.

2. Observations of the SN Site and Data Reduction

As part of our ongoing survey of M101 for massive stars we had already downloaded archival HST ACS images taken with its F435W, F555W, and F814W filters to combine with our HST Wide Field Camera 3 (WFC3) data taken with a narrowband F469N filter, tuned to the strong HeII emission line at 468.6 nm. The images were reduced using the MULTIDRIZZLE routine and mapped onto our WFC3/F469N narrowband imaging as described in Shara et al. (2013). Photometry was performed using the standalone DAOPHOT code (Stetson 1987), and a model point-spread function (PSF) based on isolated pointlike stars was built and applied to all other stars in the field. Zero-points from the HST literature were applied to convert our observed magnitudes into Vega magnitudes using the ACS Zero-point Calculator webtool.[3]

Using the methods outlined in Shara et al. (2013) we determine our photometric detection limit for the F435W image to be $m_{\rm F435W} = 28.5$ mag; although this is the faintest object we can detect, we do not always do so with 100% efficiency. The magnitude at which we are confident we will always detect an object, our 100% detection limit, is $m_{\rm F435W} = 26.7$ mag. Using the extinction law of Cardelli et al. (1989) and assuming an average extinction of $A(\rm H\alpha)$=1.06 mag and a Milky Way

[3] The Zero-point Calculator is available at https://www.stsci.edu/hst/instrumentation/acs/data-analysis/zeropoints.

Table 1
Archival HST ACS/WFC Data Used for Progenitor Identification with the Detection Limits Given in Vega Magnitudes

Filter	Date Obs	Exposure Time (s)	Faintest Limit	A_λ	100% Detection Limit	
					Apparent	Absolute
F435W	2002 Nov 15	1620	28.5	1.74	26.7	−4.07
F555W	2002 Nov 16	1440	28.0	1.36	26.6	−3.79
F814W	2002 Nov 16	1440	27.3	0.80	25.8	−4.03

Note. All data were obtained under program ID 9490 (PI: Kuntz).

Table 2
Four H II Regions Close to the Site of SN 2023ixf

ID	C(Hβ)	$E(B–V)$	A_{F814W}	R_{23}	$12 + \log(O/H)_{lower}$	$12+\log(O/H)_{upper}$
1105	0.36	0.277	0.413	6.01	7.58	8.53
1098	0.74	0.570	0.849	4.50	7.40	8.63
1086	0.32	0.246	0.362	5.02	7.47	8.59
1052	0.29	0.223	0.332	5.22	7.49	8.58
Average	0.428	0.329	0.490	5.188	7.485	8.583

Note. Hβ and R_{23} are taken from Kennicutt & Garnett (1996), and we note ID names correspond to those in Hodge et al. (1990).

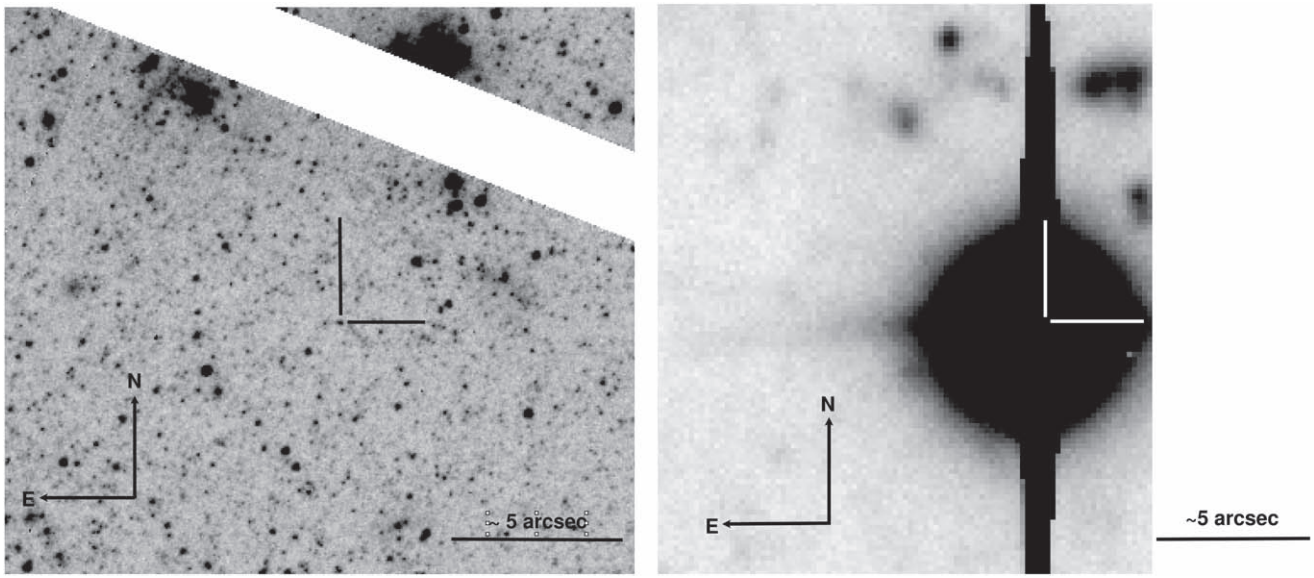

Figure 1. HST/ACS F814W image taken in 2002 November (left) and Gemini/GMOS *r*-band image taken in 2023 June (right) at the site of SN 2023ixf in M101, which became available after the initial submission of this Letter. The location of the SN is highlighted and is coincident with a single source in the F814W image. We note the SN is on the edge of one of the GMOS-N chips.

foreground reddening of $E(B–V) = 0.01$ mag (Lee et al. 2009), corresponding to $A_{F435W} = 1.74$ mag, we determine our absolute magnitude 100% detection limit to be $M_{F435W} = -4.07$ mag. The mean Galactic extinction curve does not work well for other galaxies, especially with high star formation rates like M101 (Calzetti et al. 1994), so we use values from Pang et al. (2016) for A_{F555W} and A_{F814W}, which are presented along with completeness limits for each filter in Table 1.

While average extinction values are useful to determine our detection limit for objects in M101, more local values of extinction are required for analysis of the progenitor region and ultimately the determination of the initial mass. The SN site lies $\sim 1''$ from the H II region NGC 5461, which has undergone analysis by Kennicutt & Garnett (1996), who analyzed spectra of regions 1105, 1098, 1086, and 1052 shown in their Figure 2(b). While these may not be representative of the exact SN site they are the closest available in the published literature. In Table 2 we present C(Hβ) and R_{23} values from Table 2 in Kennicutt & Garnett (1996) and determine $A_{F814W} = 0.49^{+0.359}_{-0.158}$. We note that the R_{23} indicator is double-valued and thus we use the calibration from equation (8) in Yin et al. (2007) to calculate the lower branch 12+log(O/H) and Pilyugin & Thuan (2005) with an excitation parameter $P = 0.9$ for the upper branch. Metallicities derived from these equations for each of the four H II regions local to the SN site are presented in Table 2. The average metallicity is $12 + \log(O/H) = 7.485$ for the lower branch and $12 + \log(O/H) = 8.583$ for the upper branch. We note that no Hα fluxes are presented in Kennicutt & Garnett (1996), so the O3N2 or N2 calibrators from e.g., Pettini & Pagel (2004) cannot be used. However, metallicity determinations of other nearby H II regions, albeit further from

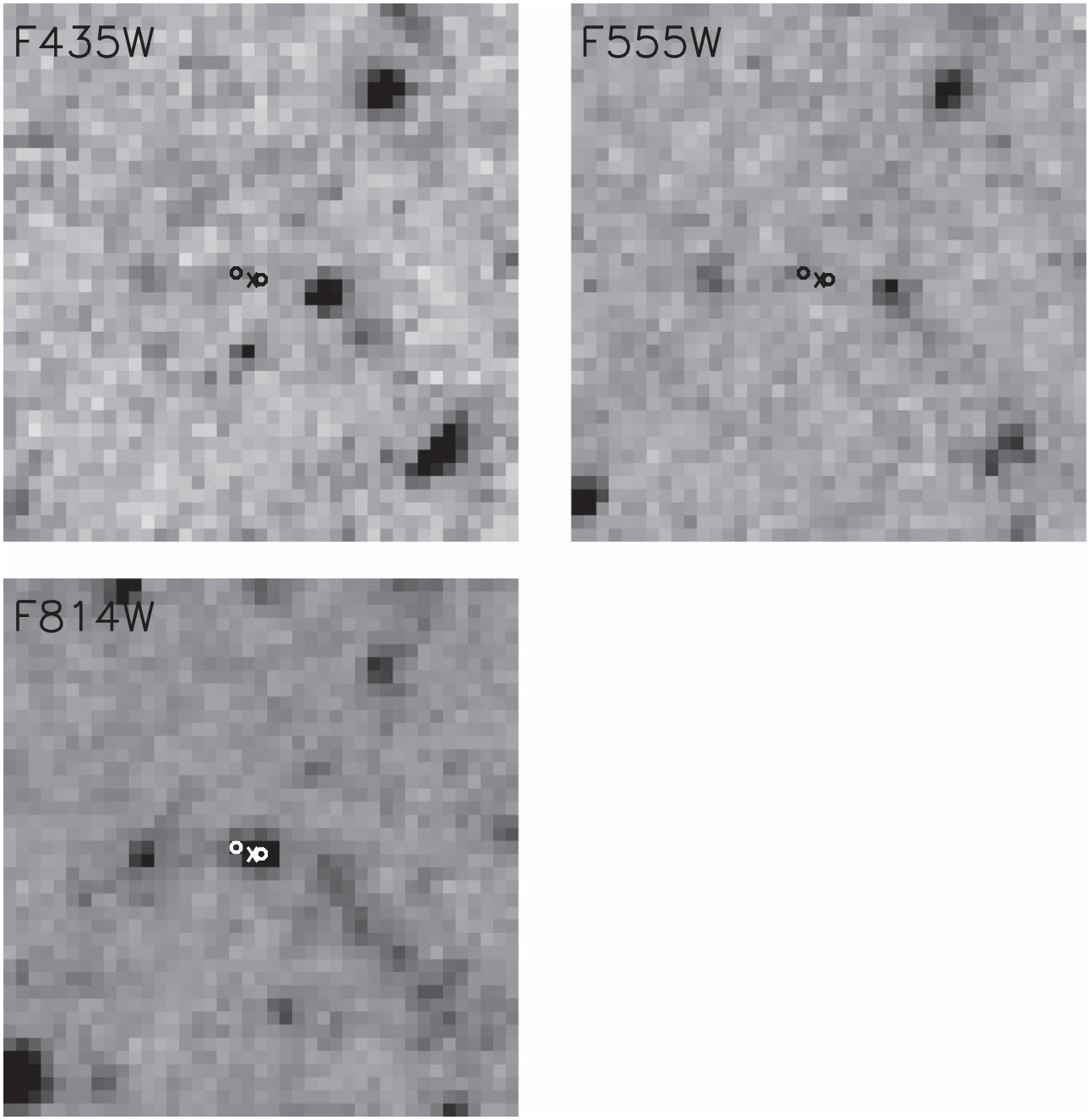

Figure 2. Hubble Space Telescope ACS/WFC images of the $\sim$2 arcsec^2 region around the site of SN 2023ixf in F435W (top left), F555W (top right), and F814W (bottom) filters. The location of the two sources identified in the F814W image are marked with a circle (with the size corresponding to 1σ positional error), while the SN location is indicated by a cross. We note that north is up and east is left.

the SN site, presented in Pledger et al. (2018) using the O3N2 calibration suggests the upper branch is more likely.

3. Identification of the SN Progenitor

To identify any potential progenitors of SN 2023ixf we must compare the location of the SN with pre-SN imaging that in turn requires a consistent coordinate system between the images. From our previous work our HST images in the three different filters have already been aligned using a geometric transformation from the GEOMAP routine within the HST MULTIDRIZZLE software (Shara et al. 2013). We applied the same method to *r*-band Gemini/GMOS-N observations of SN 2023ixf (PI: Lotz, Program ID: GN-2003A-DD-105) taken on 2023 June 5. We compared the positions of 30 sources common to both images that yielded a geometric transformation of the Gemini image onto the F814W/ACS image with an rms error of $\pm$ 24 mas. We applied this transformation using GEOTRAN, and then compared coordinates of our targets again, finding a standard deviation of $\sigma = 0\farcs03$. The SN in the 60 s exposure was saturated, which made identifying the center of the SN source difficult. To negate this we combined several 1 s *g*-, *r*-, and *i*-band GMOS images and repeated the same geometric transformation procedure finding a slightly higher standard deviation of $0\farcs07$ as a result of the reduced number of common sources. The center of the SN was then identified using the mean X and Y profile function in GAIA, which was

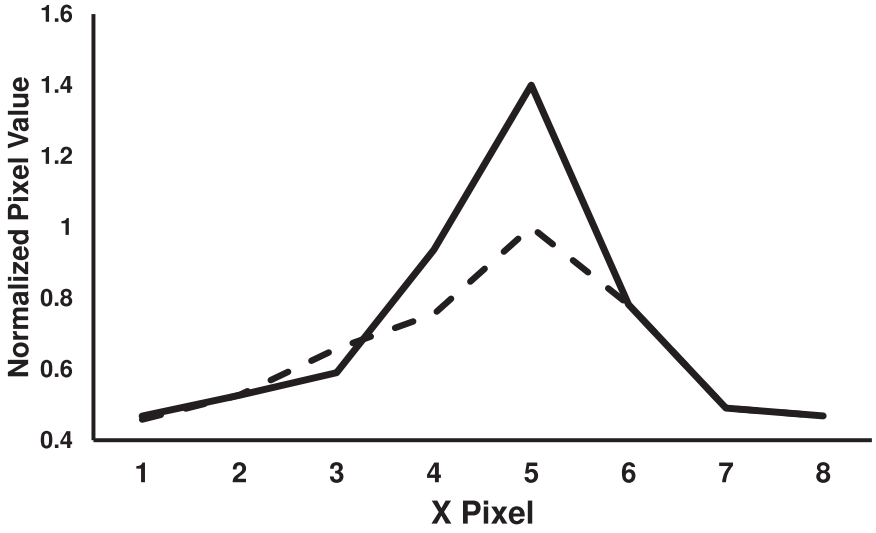

Figure 3. Mean x-profile of the source at the location of SN 2023ixf (dashed line), and for comparison the mean x-profile of a nearby pointlike star (solid line). The peak at $x \sim 5$ corresponds to the brightest part of the source, and another peak is suggested at $x \sim 3$ for the second, fainter source that is not seen in the comparison star.

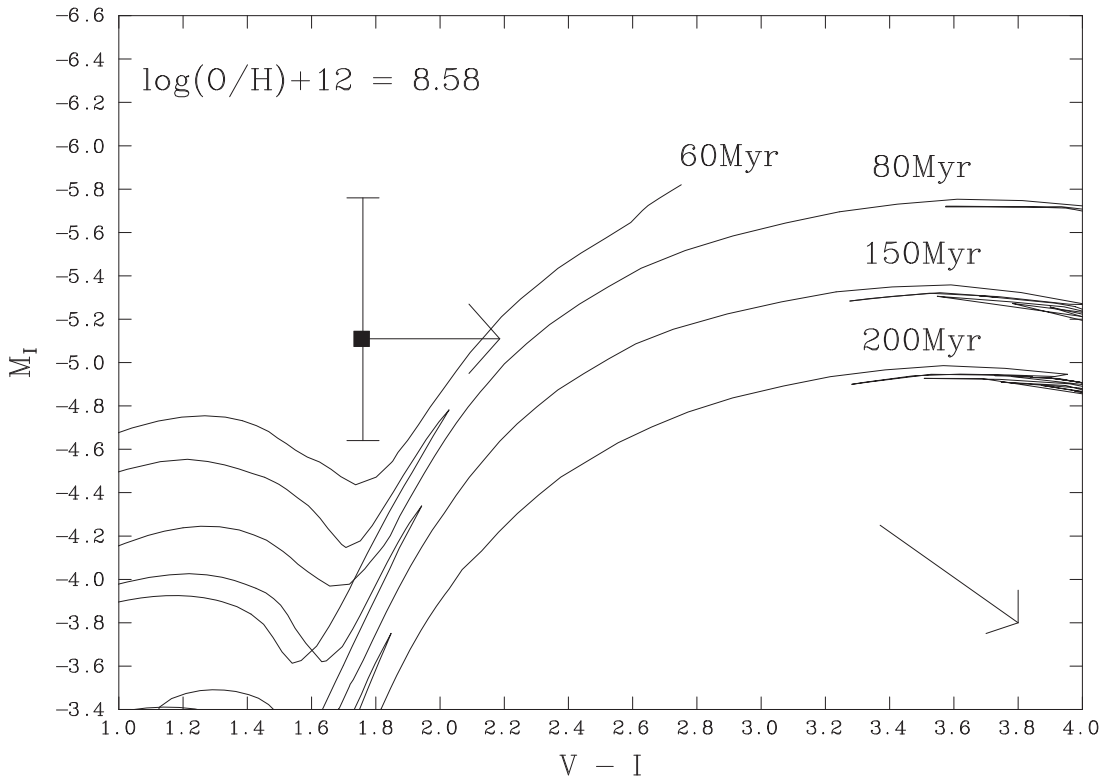

Figure 4. Color–magnitude diagram plotting 80–200 Myr PARSEC stellar evolutionary isochrones along with our progenitor candidate at a metallicity of log(O/H) + 12 = 8.58. The *V–I* plotted is a lower limit using the 100% detection limit of our F555W images, and as such we expect the true value to be farther to the right in this plot. We also note that the star will explode at the end of the evolutionary track. The reddening vector to show the effect of extinction is plotted in the lower right corner

in agreement with the DAOPHHOT routines in IRAF to within ±35 mas. This allowed us to determine an accurate position for the SN in the archival imaging as shown in Figure 1.

Using this position and error we detected no progenitor in the F435W image, with the nearest source ∼0.″44 to the southwest of the supernova location. The F555W image also shows no obvious photometric detection, though one could argue at a hint of a source at the detection limit but slightly off-center from the SN location as shown in Figure 2. Unfortunately our WFC3/F469N images just miss the SN site; however, a Type II progenitor would not be expected to be a star with strong helium emission such as a Wolf–Rayet star.

The F814W image reveals a source coincident with the SN location, within our positional error limit (Figure 2). Inspection of the profile of the source reveals an asymmetric profile as shown in Figure 3 suggesting that the source is two partially resolved stars that would be consistent with the hint of an offset

source in the F555W image. This is further supported from comparison with a nearby pointlike star that does not show any evidence of an asymmetric profile. At a distance of 6.4 Mpc, the 0.″15 spatial resolution of our drizzled HST/ACS images corresponds to a physical size of 4.65 pc that could easily hide multiple stars. However, our positional error suggests that the more prominent source in F814W is coincident with the SN site within 1σ, whereas the fainter, more easterly source is farther away; even taking our more conservative positional error the fainter source is still outside of the SN location.

Our photometry of these two partially unresolved sources shows that the westerly source (located at $\alpha = 14{:}03{:}38.544$ and $\delta = 54{:}18{:}41.90$) has an apparent Vega magnitude of $m_{\rm F814W} = 24.41 \pm 0.06$ mag, which assuming our average extinction $A_{\rm F814W} = 0.49^{+0.359}_{-0.158}$ mag from Table 2 and a distance of 6.4 ± 0.7 Mpc (Shappee & Stanek 2011), corresponds to an absolute magnitude of $M_{\rm F814W} = -5.11^{+0.65}_{-0.47}$ mag. Following the initial submission of this Letter we note that Soraisam et al. (2023a) find an apparent magnitude of $m_{\rm F814W} = 24.39 \pm 0.08$ mag consistent with ours and that Jacobson-Galan et al. (2023) find $E(B–V) = 0.033$ mag for SN 2023ixf based on optical spectra and fitting of the NaI D absorption line, which would be most consistent with the lower end of our absolute magnitude ($M_{\rm F814W} = -4.66$ mag). The other possible progenitor is the eastern source (located at $\alpha = 14{:}03{:}38.552$ and $\delta = 54{:}18{:}41.90$). It is not resolved well enough for a magnitude to be determined.

4. Mass Estimate

To determine a mass estimate for the progenitor we used PARSEC[4] stellar evolutionary isochrones with ages 50–200 Myr from Bressan et al. (2012). We ran models based on both our upper and lower metallicity values using our average extinction value of $A_{\rm F814W} = 0.49$ mag and used our absolute F814W magnitude of -5.11 mag, assuming a lower limit of $V–I \sim 2.2$ mag based on our 100% detection limit in F555W of 26.6 mag to assess the initial mass of the progenitor. Error bars shown in Figure 4 are based on errors in distance, extinction, and magnitude. Figure 4 shows the stellar evolutionary tracks that best match our observations assuming a metallicity of log (O/H)+12 = 8.58. Within our error bars the progenitor star is ∼60–200 Myr old, which corresponds to an initial mass of ∼4–7 $M_\odot$ given the star would explode at the end of the track. We note that stars in the lower end of this mass range would not be expected to explode as a red supergiant (RSG). Similarly, if we assume the lower metallicity of log(O/H) + 12 = 7.49 then the luminosity falls below that expected to explode as an RSG, consistent with a comparison with BPASS models (J. Eldridge 2023, private communication; Stanway & Eldridge 2018). We propose that the likely explanation for this low mass is that there is a lot of dust that we do not account for and that the progenitor's true initial mass is in the lower mass range for an RSG of 8–10 $M_\odot$. The presence of dust is consistent with the findings of Szalai & Dyk (2023), who suggest a mass of ∼15 $M_\odot$ from Spitzer data. Further analysis of the model-dependent dust, combined with light-curve modeling, is required to fully assess the nature of the progenitor. We note that this work by several groups including Soraisam et al. (2023b), who analyze JHK data from Spitzer and confirm a pulsating RSG progenitor for SN 2023ixf but determine a higher mass of ∼20 $M_\odot$, is already underway.

5. Conclusions

We have detected a possible optical counterpart to the progenitor of the SN II SN 2023ixf in archival HST images. The counterpart is not seen in (blue) F435W or (visible) F555W filter images, but is easily detected in (NIR) F814W images. The red color and brightness of the progenitor are consistent with it being a red supergiant of at least 7 $M_\odot$, likely higher at ∼8–10 $M_\odot$ if there is significant dust present. Indeed, Soraisam et al. (2023b) use Spitzer imaging to suggest a higher mass of ∼20 $M_\odot$.There is also an extremely faint, unresolved source that could also potentially be the progenitor of SN 2023ixf, although our astrometric calibration suggests this is unlikely, in agreement with IR data shown by Soraisam et al. (2023b) where the secondary candidate is not detected. There is a suggestion of a detection in the F555W image offset from the F814W source, but this would suggest a bluer object not typical of SN II progenitors. Post-SN imaging with HST will be crucial to confirm the disappearance of the progenitor, as is modeling of the SN light curve and the dust surrounding the supernova.

Acknowledgments

M.M.S. thanks James Garland for alerting him to this nearby supernova. We thank David Zurek for advice on magnitude system conversions and Anne Sansom for advice on stellar isochrones. We also thank Jan Eldridge for discussion of the progenitor mass in the BPASS models. Some of the data presented in this paper were obtained from the Mikulski Archive for Space Telescopes (MAST) at the Space Telescope Science Institute. The data used from HST is available at MAST at doi:10.17909/qbmp-nw13. Some of this work was supported by the generous support of the late Hilary and Ethel Lipsitz and we gratefully acknowledge them for their support. This research is based on NASA/ESA Hubble Space Telescope observations obtained at the Space Telescope Science Institute, which is operated by the Association of Universities for Research in Astronomy Inc. under NASA contract NAS5-26555. Based on observations obtained at the international Gemini Observatory, a program of NSF's NOIRLab, which is managed by the Association of Universities for Research in Astronomy (AURA) under a cooperative agreement with the National Science Foundation on behalf of the Gemini Observatory partnership: the National Science Foundation (United States), National Research Council (Canada), Agencia Nacional de Investigación y Desarrollo (Chile), Ministerio de Ciencia, Tecnología e Innovación (Argentina), Ministério da Ciência, Tecnologia, Inovações e Comunicações (Brazil), and Korea Astronomy and Space Science Institute (Republic of Korea).

Facilities: HST (ACS/WFC3), Gemini (GMOS-N).

Software: MULTIDRIZZLE (https://www.stsci.edu/~koekemoe/multidrizzle/), IRAF (Tody 1986), PARSEC isochrones are freely available from http://stev.oapd.inaf.it/.

ORCID iDs

Joanne L Pledger https://orcid.org/0000-0001-8907-3051
Michael M Shara https://orcid.org/0000-0003-0155-2539

[4] PARSEC isochrones are freely available from http://stev.oapd.inaf.it/.

References

Baade, W., & Zwicky, F. 1934, PNAS, 20, 259
Bertola, F. 1964, AnAp, 27, 319
Blandford, R. D., & Ostriker, J. P. 1978, ApJL, 221, L29
Bressan, A., Marigo, P., Girardi, L., et al. 2012, MNRAS, 427, 127
Burbidge, E. M., Burbidge, G. R., Fowler, W. A., & Hoyle, F. 1957, RvMP, 29, 547
Calzetti, D., Kinney, A. L., & Storchi-Bergmann, T. 1994, ApJ, 429, 582
Cameron, A. G. W. 1957, PASP, 69, 201
Cano, Z., Wang, S.-Q., Dai, Z.-G., & Wu, X.-F. 2017, AdAst, 2017, 8929054
Cardelli, J. A., Clayton, G. C., & Mathis, J. S. 1989, ApJ, 345, 245
Clayton, D. D. 1982, in NATO Advanced Study Institute (ASI) Series C, Vol. 90, Supernovae: A Survey of Current Research, ed. M. J. Rees & R. J. Stoneham (Dordrecht: Springer), 535
Corbelli, E., & Salpeter, E. E. 1988, ApJ, 326, 551
Gilmozzi, R., Cassatella, A., Clavel, J., et al. 1987, Natur, 328, 318
Grefenstette, B. 2023, ATel, 16049, 1
Hodge, P. W., Gurwell, M., Goldader, J. D., & Kennicutt, R. C. J. 1990, ApJS, 73, 661
Hoyle, F., & Wickramasinghe, N. C. 1970, Natur, 226, 62
Itagaki, K. 2023, TNSTR, 2023-39, 1
Jacobson-Galan, W. V., Dessart, L., Margutti, R., et al. 2023, arXiv:2306.04721
Johnson, J. A., Fields, B. D., & Thompson, T. A. 2020, RSPTA, 378, 20190301
Kawai, N., Serino, M., Negoro, H., et al. 2023, ATel, 16044, 1
Kennicutt, R. C. J., & Garnett, D. R. 1996, ApJ, 456, 504
Langer, N. 2012, ARA&A, 50, 107
Lee, J. C., Gil de Paz, A., Tremonti, C., et al. 2009, ApJ, 706, 599
Liu, Z.-W., Roepke, F. K., & Han, Z. 2023, RAA, 23, 43
McKee, C. F., & Cowie, L. L. 1975, ApJ, 195, 715
Pang, X., Pasquali, A., & Grebel, E. K. 2016, AJ, 151, 23
Perley, D., Meynardie, W., Chu, M., & Fremling, C. 2023, TNSCR, 2023-146, 1
Perlmutter, S., Aldering, G., Goldhaber, G., et al. 1999, ApJ, 517, 565
Pettini, M., & Pagel, B. E. J. 2004, MNRAS, 348, L59
Pilyugin, L. S., & Thuan, T. X. 2005, ApJ, 631, 231
Pledger, J. L., Shara, M. M., Wilde, M., et al. 2018, MNRAS, 473, 148
Riess, A. G., Filippenko, A. V., Challis, P., et al. 1998, AJ, 116, 1009
Rodríguez, Ó. 2022, MNRAS, 515, 897
Shappee, B. J., & Stanek, K. Z. 2011, ApJ, 733, 124
Shara, M. M., Bibby, J. L., Zurek, D., et al. 2013, AJ, 146, 162
Smartt, S. J. 2009, ARA&A, 47, 63
Soraisam, M., Matheson, T., Andrews, J., et al. 2023a, ATel, 16050, 1
Soraisam, M. D., Szalai, T., Van Dyk, S. D., et al. 2023b, arXiv:2306.10783
Stanway, E. R., & Eldridge, J. J. 2018, MNRAS, 479, 75
Stetson, P. B. 1987, PASP, 99, 191
Sukhbold, T., Ertl, T., Woosley, S. E., Brown, J. M., & Janka, H. T. 2016, ApJ, 821, 38
Szalai, T., & Dyk, S. V. 2023, ATel, 16042, 1
Thwaites, J., Vandenbroucke, J., Santander, M. & IceCube Collaboration 2023, ATel, 16043, 1
Tinsley, B. M. 1975, PASP, 87, 837
Tody, D. 1986, Proc. SPIE, 627, 733
Van Dyk, S. D. 2017, RSPTA, 375, 20160277
Villafane, J., Nespral, D., Zamora, O., et al. 2023, ATel, 16045, 1
Williams, B. F., Hillis, T. J., Blair, W. P., et al. 2019, ApJ, 881, 54
Yin, S. Y., Liang, Y. C., Hammer, F., et al. 2007, A&A, 462, 535
Zwicky, F. 1964, ApJ, 139, 514